# Elucidating Internucleosome Interactions and the Roles of Histone Tails

Steven C. Howell,[†] Kurt Andresen,[‡] Isabel Jimenez-Useche,[§] Chongli Yuan,[§] and Xiangyun Qiu[†*]
[†]Department of Physics, George Washington University, Washington, DC; [‡]Department of Physics, Gettysburg College, Gettysburg, Pennsylvania; and [§]School of Chemical Engineering, Purdue University, West Lafayette, Indiana

ABSTRACT The nucleosome is the first level of genome organization and regulation in eukaryotes where negatively charged DNA is wrapped around largely positively charged histone proteins. Interaction between nucleosomes is dominated by electrostatics at long range and guided by specific contacts at short range, particularly involving their flexible histone tails. We have thus quantified how internucleosome interactions are modulated by salts (KCl, $MgCl_2$) and histone tail deletions (H3, H4 N-terminal), using small-angle x-ray scattering and theoretical modeling. We found that measured effective charges at low salts are ~1/5th of the theoretically predicted renormalized charges and that H4 tail deletion suppresses the attraction at high salts to a larger extent than H3 tail deletion.

## INTRODUCTION

Highly charged DNA is packaged into nucleosome core particles (NCP) in eukaryotic cells by wrapping every 147 per ~180 basepairs (bp) of DNA around a histone octamer. The octamer is a protein complex comprising two copies of each of the four histone proteins (named H2A, H2B, H3, and H4). Each histone has one C-terminal and one N-terminal tail that protrude out from the octameric core. Linked by ~20–60 bp DNA like beads on a string, NCPs are further packaged into chromatin whose conformation and dynamics underpins gene maintenance and regulation. Thus, there has been long-standing interest in physically understanding nucleosome structure and interaction fundamental to chromatin function.

Polyelectrolyte behavior and histone tail modulation are among the key determinants of the multifactorial packaging of nucleosomes (1). One NCP carries a net negative charge of ~150 $e$ with −294 $e$ from DNA and +144 $e$ from histone proteins. Given its diameter of ~10 nm and height of ~6 nm, this leads to an average charge density of $-0.43\ e/\text{nm}^2$, about half of the $-1\ e/\text{nm}^2$ of DNA. The expected polyelectrolyte behavior of NCP is demonstrated by cation-modulated unfolding and compaction of NCP arrays (2,3). Notably, divalent cations go beyond screening the electrostatic repulsion between NCPs and can mediate inter-NCP attraction, e.g., $Mg^{2+}$- or $Ca^{2+}$-induced condensation of mono- and polynucleosomes (4). In contrast, these divalent cations are unable to condense DNA. This suggests significant roles of the complex charge distribution of NCP furnished by the histones (5). In particular, the tails of histones (~30% of the histone mass), being highly positively charged and flexible, are known to be crucial in modulating nucleosome interaction and chromatin assembly (1).

There have been extensive experimental studies aiming to elucidate the electrostatics of nucleosomes and the roles of histone tails. The effects of cations of varied valences on the nucleosome assembly have been well characterized (1–3,6), e.g., by measuring the sedimentation coefficients of nucleosome arrays or the fraction of condensed nucleosomes (4,7). Among the 16 histone tails, the eight N-terminal tails hold the most positive charges and are considered more significant, e.g., NCPs with all N-terminal tails deleted remain soluble in high divalent salts (8). In an effort to dissect the contribution from each N-terminal tail, all 16 possible tail-deletion NCP mutants have been studied and it was found that all N-terminal tails contribute to the condensation of oligo-NCP arrays nonspecifically and additively (8). Still, the histone tails vary in length and charge and thus differ in strength in mediating nucleosome interactions, e.g., H3 and H4 tails, studied herein, were observed to be more important than H2A and H2B tails (8,9).

Systematic measurements have promoted widespread theoretical interests in mechanistically understanding the structure and interaction of nucleosomes (10,11). At the atomic level, enabled by the availability of high resolution crystal structures (12), molecular dynamics simulations have described the ion and solvent atmospheres of nucleosome and revealed rugged electrostatic surfaces (13,14). The flexible histone tails have been analyzed in detail and shown to display multistate conformational dynamics (15–17). At the coarse-grain level, both nucleosome arrays and chromatin have been modeled to recapture the conformational changes under varied conditions such as salt and mechanical stretching (18,19). However, to apply the detailed NCP structures and energetics predicted by theoretical approaches, stringent experimental tests are required, but largely lacking. For example, as the focus of this study, one key factor to the assembly of NCPs is the effective inter-NCP potential that is usually computed following the Poisson-Boltzmann formulism for efficiency (11). However, such theoretical treatment has not been validated experimentally due to the lack of direct measurements of inter-NCP potentials. Comparisons with previously measured

*Submitted December 16, 2012, and accepted for publication May 6, 2013.*

*Correspondence: xqiu@gwu.edu

Editor: Gerhard Hummer.



0006-3495/13/07/0194/6 $2.00

http://dx.doi.org/10.1016/j.bpj.2013.05.021

quantities are often difficult, e.g., the interpretation of sedimentation coefficient necessitates an ab initio hydrodynamic model.

Here, we report measurements of interactions between monomeric nucleosomes using solution small-angle x-ray scattering (SAXS) in conjunction with theories of polyelectrolytes. There are two outcomes we deem important: 1), Quantification of inter-NCP pair potentials by modeling full SAXS profiles; 2), Elucidation of the individual role of H3 and H4 tails. Although SAXS (and small-angle neutron scattering for neutron) has been used to study the structure and interaction of NCPs since the 1970s (20), no quantitative refinement of full SAXS profiles has been done to extract the inter-NCP interactions, which we obtain here by refining synchrotron SAXS data. One key advantage of full profile modeling is quantification of the inter-NCP potential as a function of inter-NCP distance (21), in contrast to single-parameter measurements such as second virial coefficients or osmotic pressures of NCP solutions. Bertin et al. (22) have compared full SAXS profiles with theoretical calculations. However, refinements were not performed, possibly due to the relatively dilute NCP concentrations ($\leq$ 8 mg/ml, ~0.04 mM) and limited angular range of the in-house SAXS data that lower SAXS sensitivity to inter-NCP interactions. In addition, using recombinant NCP constructs with either H3 or H4 tail deleted, to the best of our knowledge we report the first analysis of this kind on the respective role of H3 and H4 tails in mediating inter-NCP interactions.

## MATERIAL AND METHODS

Natural-source monomeric NCPs (NS-NCP) were prepared from adult chicken erythrocytes as in (23). Gel electrophoresis was used to assess the DNA length (147 $\pm$ 5 bps) and the histone content (Fig. S1, *a* and *b*, in the Supporting Material). Recombinant nucleosomes (RC-NCP) were reconstituted by mixing 147-bp mouse mammary tumor virus DNA and histone octamers with sequences from *Xenopus laevis* following standard protocols (8) (Fig. S1, *a* and *c*). The globular H3 and H4 recombinant proteins were truncated at their N-terminal ends (referred to as gH3 and gH4 RC-NCPs), by deleting the coding sequences of amino acids (1–27 with +10 *e* of H3 and 1–10 with +3 *e* of H4) via site-directed mutagenesis. All NCP stocks were purified by size-exclusion chromatography (Sephacryl S300-HR medium) and then dialyzed against 10 mM KCl 10 mM Tris 0.1 mM EDTA pH 7.5 buffer. Salts were adjusted to studied conditions by adding concentrated salts. SAXS experiments were carried out at 20°C at the G1 station at the Cornell High Energy Synchrotron Source in Ithaca, New York. The incident beam had an energy of 9.97 keV and size of 250 $\times$ 250 $\mu$m. Samples of ~30 $\mu$l were injected into an in-vacuum capillary flow cell to enable windowless data collection for background reduction. Radiation damage was mitigated by optimizing x-ray exposure time and oscillating the plug of sample solution. Six to eight two-second exposures of the same sample were taken and verified to be reproducible, indicative of the absence of radiation damage.

## RESULTS

Measured SAXS profile I(Q) is a product of the form factor P(Q) and the structure factor S(Q), i.e., I(Q) = P(Q) $\times$ S(Q), with S(Q) becoming significant under conditions such as high [NCP]s and strong inter-NCP interactions. I(Q) of a dilute NCP solution (i.e., S(Q) = 1) thus measures the structure of individual NCPs in terms of the form factor P(Q) = I(Q). This can reveal differences between molecular structures in solution and in crystal. Fig. 1 shows excellent agreement between the SAXS profile measured in solution and the profile calculated from a crystal structure in Q range of 0.01–0.28 Å$^{-1}$, indicative of high sample purify and structural conformity. The same level of agreement was observed for all NCP constructs (i.e., NS-NCP, wild-type, gH3, and gH4 RC-NCPs). It is worth noting that the crystal structure P(Q) shows an extra dip around Q of 0.14 Å$^{-1}$. This discrepancy has been observed in previous reports (22,24) and was attributed to the DNA unwrapping at the ends by a few basepairs. Tail deletions lead to small changes of the dip around Q = 0.14 Å$^{-1}$ that can be attributed to increased DNA unwrapping (data not shown). Nonetheless, these dips appear in relatively high Q and do not affect our subsequent analysis. Guinier analysis of the low Q data (Fig. 1, *inset*) gives the radius of gyration $R_g$ = 44.4 (3) Å, which is nearly identical to previous SAXS measurements of natural-source NCPs (25) and recombinant NCPs with $\alpha$-satellite DNA (24). Note that NCPs reconstituted with the 601 sequence were reported to give slightly smaller $R_g$ by 2–3 Å (22,24).

In addition to structure information, SAXS is capable of quantifying intermolecular interactions, via the structure factor S(Q) originating from spatial correlations between molecules. Qualitatively, repulsive interaction leads to a decrease of low Q intensities, i.e., a downturn, and attractive interaction gives rise to an increase at low Q, i.e., an upturn. Fig. 2 shows how SAXS profiles evolve with NCP and salt concentrations. As expected from strong inter-NCP

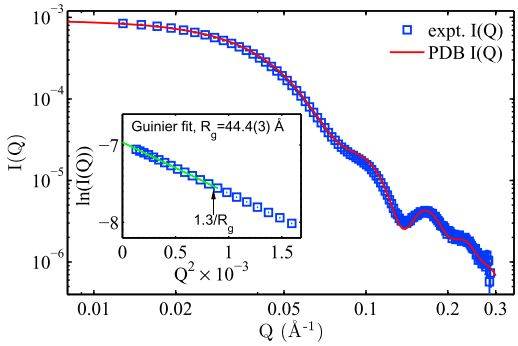


FIGURE 1 SAXS form factor P(Q) of NS-NCP from experiment (□) and crystal structure (*red*, PDB ID: 1KX5). Q = 4$\pi$sin($\theta$)/$\lambda$ is the scattering vector, where 2$\theta$ is the scattering angle and $\lambda$ is the x-ray wavelength. The experiment form factor was measured at a dilute NCP concentration of 0.003 mM (~0.6 mg/ml) and an intermediate salt (40 mM KCl) to minimize the influence of inter-NCP interferences. Error bars of I(Q)s, in this and subsequent plots, are smaller than symbol sizes except at high Qs. Inset shows the Guinier fit (*solid line*) to obtain the radius of gyration ($R_g$). The linear region extends well over the empirical $Q_{max}$ cutoff of 1.3/$R_g$ for globular structures.

repulsions at low salts (10 and 40 mM KCl, Fig. 2, *a* and *b*), low Q downturns are observed and deepen upon increasing [NCP]. In contrast, low Q upturns appear and heighten with [NCP] at high salts (100 and 200 mM KCl, Fig. 2, *c* and *d*), indicating inter-NCP attractions. These observations are consistent with reports of negative virial coefficients at >70 mM KCl (22). Divalent $Mg^{2+}$, known to condense NCP at >2.5 mM [$Mg^{2+}$] (4), was also studied and the onset of inter-NCP attraction was found to be between 1 and 2 mM [$Mg^{2+}$] (Fig. S3).

To gain quantitative insights into the underlying inter-NCP interactions, we then applied the generalized one component method (GOCM) with the mean spherical approximation (21,26) to model the structure factors. As both repulsion and attraction exist, the general form of inter-NCP interaction potential as a function of inter-NCP distance is given by

$$U(r) = \begin{cases} \infty & r<\sigma \\ \dfrac{Z_{\mathrm{eff}}^2}{\varepsilon(1+\kappa\sigma/2)^2}\dfrac{e^{-\kappa(r-\sigma)}}{r} - \dfrac{Z_{\mathrm{attr}}^2}{\varepsilon(1+\kappa_{\mathrm{attr}}\sigma/2)^2}\dfrac{e^{-\kappa_{\mathrm{attr}}(r-\sigma)}}{r} & r\geq\sigma \end{cases},$$

where $\sigma$ is the equivalent diameter of NCP, $Z_{\mathrm{eff}}$ and $Z_{\mathrm{attr}}$ are the effective charges to be fitted, $\varepsilon = 80.4$ is the dielectric constant of water at 20°C, and $\kappa$ is the inverse Debye screening length calculated from the salt condition. Namely, the inter-NCP potential comprises a hard-sphere (HS) repulsive term, a Debye-Huckel (DH) electrostatic repulsive term, and a DH-like attractive term. Although it is possible to include both DH potentials in the fitting procedures, there exist significant correlations between the fitted repulsive and attractive DH terms despite better fits (see the Supporting Material for detailed results and discussions). Due to this complication, the attractive DH potential is turned off (i.e., $Z_{\mathrm{attr}} = 0$) under conditions where a net inter-NCP repulsion is observed. Likewise, $Z_{\mathrm{eff}}$ is set to 0 under conditions where a net attraction is observed. As the physical origin of the attraction is poorly understood, we chose a short-range attraction of effective charge $Z_{\mathrm{attr}}$ and 4.8 Å decay length for all data. The effect of NCP's disk-like shape (axis ratio ~2) on S(Q) only becomes significant at $Q > 0.036$ Å$^{-1}$ (22) where S(Q) ~1 as observed in the experiments; it is thus not considered. Such GOCM fits are shown in Fig. 2 as solid lines, noting that the form factor for each NCP construct is calculated based on the crystal structure (shown in Fig. S2). It is evident that the GOCM fits are in good agreement with experimental data over the entire Q range. Inter-NCP interactions are thus quantified in the forms of HS and DH potentials.

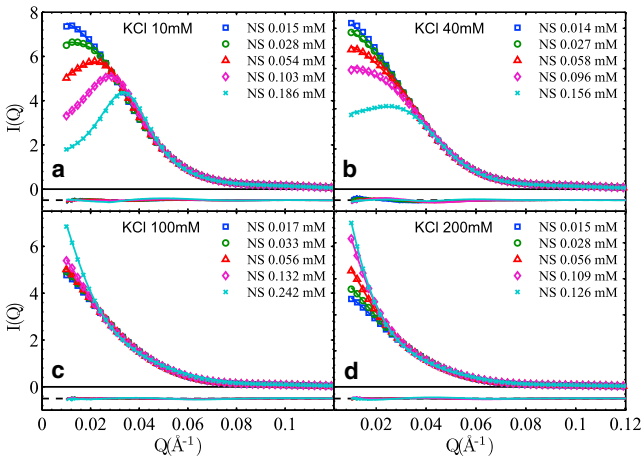


FIGURE 2 SAXS profiles, I(Q) = P(Q) × S(Q), of NS-NCPs at four KCl concentrations. I(Q)s are normalized by NCP concentrations to assist comparison. Each panel shows experimental I(Q)s (*symbols*) at a series of [NCP]s (0.1 mM gives ~20 mg/ml) as indicated in the legends, together with their respective theoretical fits (*lines*). The residues are shown with an offset at the same scale. The pertinent pair-potential parameters are (discussed in detail in the main text), (*a*) $Z_{\mathrm{eff}} = 22$ (1) e, $\sigma = 140$ Å; (*b*) $Z_{\mathrm{eff}} = 23$ (1) e, $\sigma = 110$ Å; (*c*) $Z_{\mathrm{attr}} = 150$ (5) *e*, $\sigma = 100$ Å; (*d*) $Z_{\mathrm{attr}} = 200$ (8) *e*, $\sigma = 100$ Å. Uncertainties of *Z* values originate from both curve fitting (via variance-covariance matrix, ~1%) and small variations (~3%) between values at different [NCP]s. The $Z_{\mathrm{eff}}$ and $Z_{\mathrm{attr}}$ values are poorly defined when [NCP] is small (<0.03 mM, or 6 mg/ml) and their values given here are from data at high [NCP]s.

Despite being quantitative, directly usable, and comparable with theoretical studies, it should be noted that the sum of HS and DH potentials describes an apparent inter-NCP interaction that reproduces the measured structure factor. In the case of inter-NCP repulsion, the effective charge $Z_{\mathrm{eff}}$, as the only fitting parameter, differs from the bare charge $Z_{\mathrm{bare}}$ due to the nonlinear nature of ion screening and the validity of DH potentials in linear regime only. For the same reason, the equivalent diameter $\sigma$ encloses the vicinity with a large electrostatic field (e.g., >3.8 $k_{\mathrm{B}}T/e$ was used for dsDNA by the authors (27)), which is in the order of Debye length. Especially at low salt, $\sigma$ is significantly larger than the 100 Å computed from the NCP crystal structure (21). We determined the value of $\sigma$ at different salts based on cell model numerical calculations (27,28), and the same $\sigma$ value was then fixed for all data at the same ionic condition for consistency. We show these relevant interaction potential parameters in the figure captions and in Table S1.

Fig. 3 shows data from recombinant gH3 and gH4 RCNCPs at two salt conditions (10 and 100 mM KCl) together with GOCM fits (data at 20 and 40 mM KCl are shown in Fig. S4). We primarily focused on gH3 and gH4

RC-NCPs because recombinant samples were relatively limited in volume and previous studies have reported the second virial coefficients (though no inter-NCP potentials) of intact RC-NCPs and gH3gH4 RC-NCPs, i.e., with none or both tails deleted (22). To enable cross-comparisons, intact RC-NCPs were measured at a few selected conditions (Fig. S5). At low salt of 10 mM KCl, essentially no difference in the effective charge $Z_{eff}$ (~22 $e$) was observed among all NCP constructs (i.e., NS-NCP, gH3, gH4, and intact RC-NCPs), noting that the negativity of $Z_{eff}$ is omitted for brevity. We further calculated the second virial coefficient from the inter-NCP potential using

$$A_2 = \frac{1}{2}\int_0^\infty \left(1 - e^{-U(r)/k_BT}\right)4\pi r^2 dr,$$

and obtained a value of $2.5(1) \times 10^{-4}$ ml·mol/g$^2$. This value is in excellent agreement with the osmometry measurement by Mangenot et al. (29). Bertin et al. (22) used theoretical calculations of $Z_{eff}$ between 70 and 125 $e$ and obtained much larger $A_2$ values close to $5.0 \times 10^{-4}$ ml·mol/g$^2$. We attribute the difference to the discrepancy between theoretical and experimental $Z_{eff}$ values (discussed below) used by Bertin et al. and us, respectively. At high salt of 100 mM KCl, qualitative differences were observed: NS-NCP, gH3 and intact RC-NCPs show comparable levels of attraction; whereas gH4 and gH3gH4 RC-NCPs show no attraction (including observations in (22).). This suggests the major role of H4 tail in mediating inter-NCP attractions.

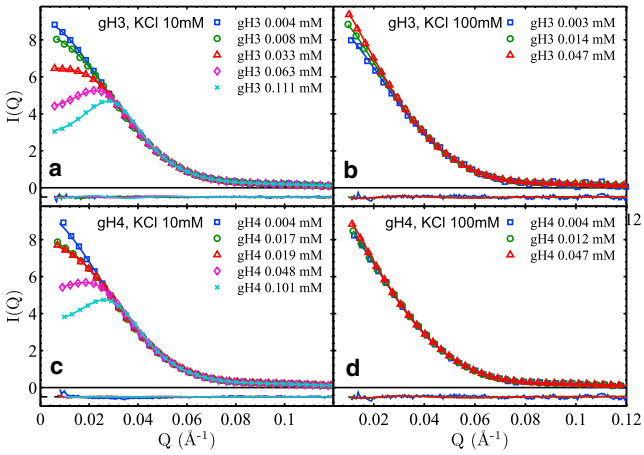


FIGURE 3 SAXS profiles, I(Q) = P(Q) × S(Q), of gH3 and gH4 RC-NCPs at 10 and 100 mM KCl. Annotations follow that of Fig. 2. Inter-NCP potential parameters are, (*a*) $Z_{eff}$ = 21 (1) $e$, $\sigma$ = 140 Å; (*b*) $Z_{attr}$ = 123 (4) $e$, $\sigma$ = 100 Å; (*c*) $Z_{eff}$ = 20 (1) $e$, $\sigma$ = 140 Å; (*d*) $Z_{attr}$ = 100 (4) $e$, $\sigma$ = 100 Å. It is worth noting that, although gH4 RC-NCP shows no interaction at 100 mM KCl, a significant $Z_{attr}$ exists so as to negate the hard sphere repulsion with $\sigma$ = 100 Å, which makes $Z_{attr}$ values artificially large. $Z_{attr}$ would be zero if $\sigma$ is zero for gH4 RC-NCP in 100 mM KCl. It is thus more appropriate to interpret $Z_{attr}$-100 as contributed by the inter-NCP short-range attraction.

## DISCUSSION

We consider the quantification of inter-NCP pair potentials from SAXS structure factors as the most interesting result of our study. Compared with the traditional analysis of second virial coefficients that relies on I(Q = 0) only, the GOCM (and methods alike) uses the full SAXS profiles and obtains self-consistent pair potentials allowing quantitative comparisons with theoretical predictions. At low salts such as 10 mM KCl, NCP-NCP interactions are dominated by repulsion as expected. Essentially the same $Z_{eff}$ is obtained for all four NCP constructs. The minimal effect of tail deletions on inter-NCP repulsion is not surprising given that tail deletions change NCP bare charges by <8% and that cations can effectively fill in for the deleted monocharged amino acids. Quantitatively, it is instructive to compare the measured $Z_{eff}$ with the theoretical renormalized charge $Z_{ren}$ that can be calculated following the charge renormalization theorem (28). For dsDNA with negatively charged groups only, our previous work showed that the measured $Z_{eff}$ is fairly consistent (within 10–25%) with its renormalized charge $Z_{ren}$ in monovalent salts (27). However, for the nucleosome, its $Z_{eff}$ (~22 $e$) is far smaller than theoretical $Z_{ren}$ (>100 $e$ for all experimental conditions), noting that $Z_{bare}$ is ~150 $e$ and $Z_{ren}$ weakly depends on NCP and salt concentrations (28). Given that the $Z_{ren}$ is calculated by treating NCP as a uniformly charged sphere, such drastic and physically significant discrepancy is likely due to the charge nonuniformity of NCP in terms of spatial distribution and sign, resulting in highly anisotropic behaviors where the uniformly charged surface consideration breaks down.

Inter-NCP interactions at short range are further complicated by the flexible histone tails (11,16). At elevated salts where electrostatic repulsion is greatly weakened, histone tail deletions can significantly affect NCP-NCP interactions. At 100 mM KCl (Fig. 2 *c*, Fig. 3, *b* and *d*), NS-NCP shows significant attraction (i.e., low Q upturn), gH3 RC-NCP shows attraction of comparable magnitude, and gH4 RC-NCP shows nearly no attraction. The difference between gH3 and gH4 RC-NCPs, which have not been studied by SAXS previously, suggests that H4 tail is more important in mediating NCP-NCP attractions than H3 tail. This corresponds well with the observed most important role of H4 tail in assembling the 30-nm chromatin fiber (7). Such trend is also consistent with the repulsion between gH3gH4 RC-NCPs up to 200 mM KCl (22). The more important role of the H4 tail in mediating internucleosome interactions has been suggested by Arya and Schlick (30) analyzing a coarse-grained mesoscale structure model with a tailored configurational-bias Monte Carlo method. As H4 tail deletion removes fewer charges than H3 tail deletion (+3 vs. +10 $e$) but shows a larger effect, this alludes to specific interactions of H4 tails with adjacent NCPs in close approach. To probe the likely H4-tail-DNA interactions, Korolev and Nordenskiöld (31) performed all-atomic

molecular dynamics simulations of DNA and H4 tails and suggested possible lysine-mediated bridging and minor groove dynamic binding. Another possible explanation is H4-tail binding with the H2A/H2B anionic patch on neighboring NCPs, as suggested by crystallography studies (32,33). This is in agreement with recent experimental studies of the effects of H4 tail lysine acetylation on nucleosome array folding that proposed site-specific lysine binding to the H2B histone (9). To fully establish the underlying molecular mechanisms, experimental approaches probing the local structure would be needed to resolve the physical origins of inter-NCP short range attraction.

## CONCLUSION

In conclusion, we have measured repulsive and attractive NCP-NCP interactions under various salt conditions with distinct NCP constructs. Quantitative knowledge of inter-NCP pair potentials should aid theoretical studies of nucleosome and chromatin high-order structure and dynamics. The physical understanding to be gained will shed light on the broad class of multiphasic macromolecules with two or more different interacting groups. Work is underway to relate the inter-NCP interactions to the conformation and energetics of nucleosome arrays through measurement and modeling.

## SUPPORTING MATERIAL

Supporting data including nine figures and one table are available at http://www.biophysj.org/biophysj/supplemental/S0006-3495(13)00577-8.

The authors thank Arthur Woll, Richard Gillian, Soren Nielsen, and Qi Xia for assistance with experiment, and thank Yun Liu for discussions on data modeling. C.Y. acknowledges Prof. Timothy Richmond (ETH, Zurich) for generously providing us the plasmids of histone proteins and MMTV DNA.

This work was supported by George Washington University (to X.Q.), Research Corporation for Science Advancement and Gettysburg College (to K.A.), and the Purdue University (to C.Y.).

## REFERENCES

1. Hansen, J. C. 2002. Conformational dynamics of the chromatin fiber in solution: determinants, mechanisms, and functions. *Annu. Rev. Biophys. Biomol. Struct.* 31:361–392.
2. Clark, D. J., and T. Kimura. 1990. Electrostatic mechanism of chromatin folding. *J. Mol. Biol.* 211:883–896.
3. Korolev, N., A. Allahverdi, …, L. Nordenskiöld. 2010. Electrostatic origin of salt-induced nucleosome array compaction. *Biophys. J.* 99:1896–1905.
4. de Frutos, M., E. Raspaud, …, F. Livolant. 2001. Aggregation of nucleosomes by divalent cations. *Biophys. J.* 81:1127–1132.
5. Sun, J., Q. Zhang, and T. Schlick. 2005. Electrostatic mechanism of nucleosomal array folding revealed by computer simulation. *Proc. Natl. Acad. Sci. USA.* 102:8180–8185.
6. Widom, J. 1998. Structure, dynamics, and function of chromatin in vitro. *Annu. Rev. Biophys. Biomol. Struct.* 27:285–327.
7. Dorigo, B., T. Schalch, …, T. J. Richmond. 2003. Chromatin fiber folding: requirement for the histone H4 N-terminal tail. *J. Mol. Biol.* 327:85–96.
8. Gordon, F., K. Luger, and J. C. Hansen. 2005. The core histone N-terminal tail domains function independently and additively during salt-dependent oligomerization of nucleosomal arrays. *J. Biol. Chem.* 280:33701–33706.
9. Allahverdi, A., R. Yang, …, L. Nordenskiöld. 2011. The effects of histone H4 tail acetylations on cation-induced chromatin folding and self-association. *Nucleic Acids Res.* 39:1680–1691.
10. Schlick, T., J. Hayes, and S. Grigoryev. 2012. Toward convergence of experimental studies and theoretical modeling of the chromatin fiber. *J. Biol. Chem.* 287:5183–5191.
11. Korolev, N., Y. Fan, …, L. Nordenskiöld. 2012. Modelling chromatin structure and dynamics: status and prospects. *Curr. Opin. Struct. Biol.* 22:151–159.
12. Richmond, T. J., and C. A. Davey. 2003. The structure of DNA in the nucleosome core. *Nature.* 423:145–150.
13. Gan, H. H., and T. Schlick. 2010. Chromatin ionic atmosphere analyzed by a mesoscale electrostatic approach. *Biophys. J.* 99:2587–2596.
14. Materese, C. K., A. Savelyev, and G. A. Papoian. 2009. Counterion atmosphere and hydration patterns near a nucleosome core particle. *J. Am. Chem. Soc.* 131:15005–15013.
15. Potoyan, D. A., and G. A. Papoian. 2011. Energy landscape analyses of disordered histone tails reveal special organization of their conformational dynamics. *J. Am. Chem. Soc.* 133:7405–7415.
16. Arya, G., and T. Schlick. 2009. A tale of tails: how histone tails mediate chromatin compaction in different salt and linker histone environments. *J. Phys. Chem. A.* 113:4045–4059.
17. Mühlbacher, F., H. Schiessel, and C. Holm. 2006. Tail-induced attraction between nucleosome core particles. *Phys. Rev. E Stat. Nonlin. Soft Matter Phys.* 74:031919.
18. Diesinger, P. M., and D. W. Heermann. 2009. Depletion effects massively change chromatin properties and influence genome folding. *Biophys. J.* 97:2146–2153.
19. Kulić, I. M., and H. Schiessel. 2003. Chromatin dynamics: nucleosomes go mobile through twist defects. *Phys. Rev. Lett.* 91:148103.
20. Hjelm, R. P., G. G. Kneale, …, K. Ibel. 1977. Small angle neutron scattering studies of chromatin subunits in solution. *Cell.* 10:139–151.
21. Chen, S. H., E. Y. Sheu, …, H. Hoffmann. 1988. Small-angle neutron-scattering investigation of correlations in charged macromolecular and supramolecular solutions. *J. Appl. Cryst.* 21:751–769.
22. Bertin, A., M. Renouard, …, D. Durand. 2007. H3 and H4 histone tails play a central role in the interactions of recombinant NCPs. *Biophys. J.* 92:2633–2645.
23. Yager, T. D., and K. E. van Holde. 1984. Dynamics and equilibria of nucleosomes at elevated ionic strength. *J. Biol. Chem.* 259:4212–4222.
24. Yang, C., M. J. van der Woerd, …, K. Luger. 2011. Biophysical analysis and small-angle X-ray scattering-derived structures of MeCP2-nucleosome complexes. *Nucleic Acids Res.* 39:4122–4135.
25. Mangenot, S., A. Leforestier, …, F. Livolant. 2002. Salt-induced conformation and interaction changes of nucleosome core particles. *Biophys. J.* 82:345–356.
26. Liu, Y., E. Fratini, …, S.-H. Chen. 2005. Effective long-range attraction between protein molecules in solutions studied by small angle neutron scattering. *Phys. Rev. Lett.* 95:118102.
27. Qiu, X., L. W. Kwok, …, L. Pollack. 2006. Measuring inter-DNA potentials in solution. *Phys. Rev. Lett.* 96:138101.
28. Trizac, E., L. Bocquet, …, H. H. von Grunberg. 2003. Alexander's prescription for colloidal charge renormalization. *Langmuir.* 19:4027–4033.

29. Mangenot, S., E. Raspaud, …, F. Livolant. 2002. Interactions between isolated nucleosome core particles: a tail-bridging effect? *Eur. Phys. J. E.* 7:221–231.

30. Arya, G., and T. Schlick. 2006. Role of histone tails in chromatin folding revealed by a mesoscopic oligonucleosome model. *Proc. Natl. Acad. Sci. USA.* 103:16236–16241.

31. Korolev, N., and L. Nordenskiöld. 2007. H4 histone tail mediated DNA-DNA interaction and effects on DNA structure, flexibility, and counterion binding: a molecular dynamics study. *Biopolymers.* 86:409–423.

32. Dorigo, B., T. Schalch, …, T. J. Richmond. 2004. Nucleosome arrays reveal the two-start organization of the chromatin fiber. *Science.* 306:1571–1573.

33. Luger, K., A. W. Mäder, …, T. J. Richmond. 1997. Crystal structure of the nucleosome core particle at 2.8 A resolution. *Nature.* 389:251–260.

Supplemental data for "**Elucidating inter-nucleosome interactions and their roles of histone tails**"

Steven C. Howell[1], Kurt Andresen[2], Isabel Jimenez-Useche[3], Chongli Yuan[3], and Xiangyun Qiu[1,*]

[1] Department of Physics, George Washington University, Washington, DC, 20052, USA;
[2] Department of Physics, Gettysburg College, Gettysburg, PA, 17325, USA;
[3] School of Chemical Engineering, Purdue University, West Lafayette, IN, 47907, USA
* To whom correspondence should be addressed. Tel: 001.202.994.6537; Fax: 001.202.994.3001; Email: xqiu@gwu.edu

## I. Supporting data to the results presented in the main text

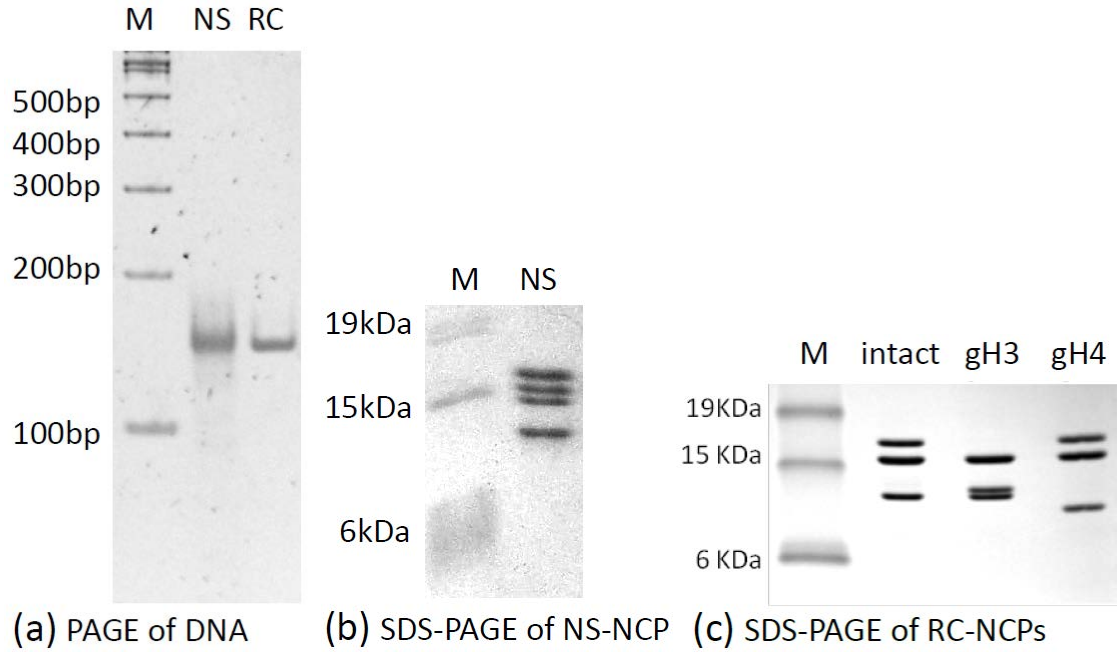


Figure S1. Characterization of nucleosome samples. (a) Extracted DNA from natural-source (NS) nucleosomes and the recombinant (RC) 147-base-pair (bp) mouse mammary tumor virus DNA in 5% polyacrylamide gel electrophoresis (PAGE). The "M" lane is the 100-bp DNA marker (Invitrogen). By analyzing the intensity distribution of each band, we obtained the full widths at half maximum (FWHM) of the bands in unit of pixels as, 100-bp marker: 10, 200-bp marker: 7.5, NS-DNA: 15, RC-DNA: 10.5. Given the distance between 100-bp and 200-bp markers are ~100 pixels, the additional smearing of the NS-DNA band is estimated to be ~10 pixels in FWHM, corresponding to ±5 base pairs. The maximum peak positions for NS-DNA and RC-DNA are identical within experimental error, noting that the NS-DNA band intensity

distribution is skewed toward longer DNA lengths as expected from the nucleosomal hindrance of Micrococcal nuclease digestion. We thus estimated the NS-DNA to be 147±5 bps. (b) Sodium dodecyl sulfate polyacrylamide gel electrophoresis (SDS-PAGE, 15%) of natural-source NCP histones. The "M" lane is the protein marker (Invitrogen BenchMark$^{TM}$). (c) SDS-PAGE of recombinant NCP histones ("intact" refers to the RC-NCP with all histone tails). Note that the recombinant H2A and H2B histones migrate as one band, while the H2A and H2B histones from NS-NCPs are well separated (b). Possible explanations include sequence differences and post-translational modifications in NS-NCP histones only.

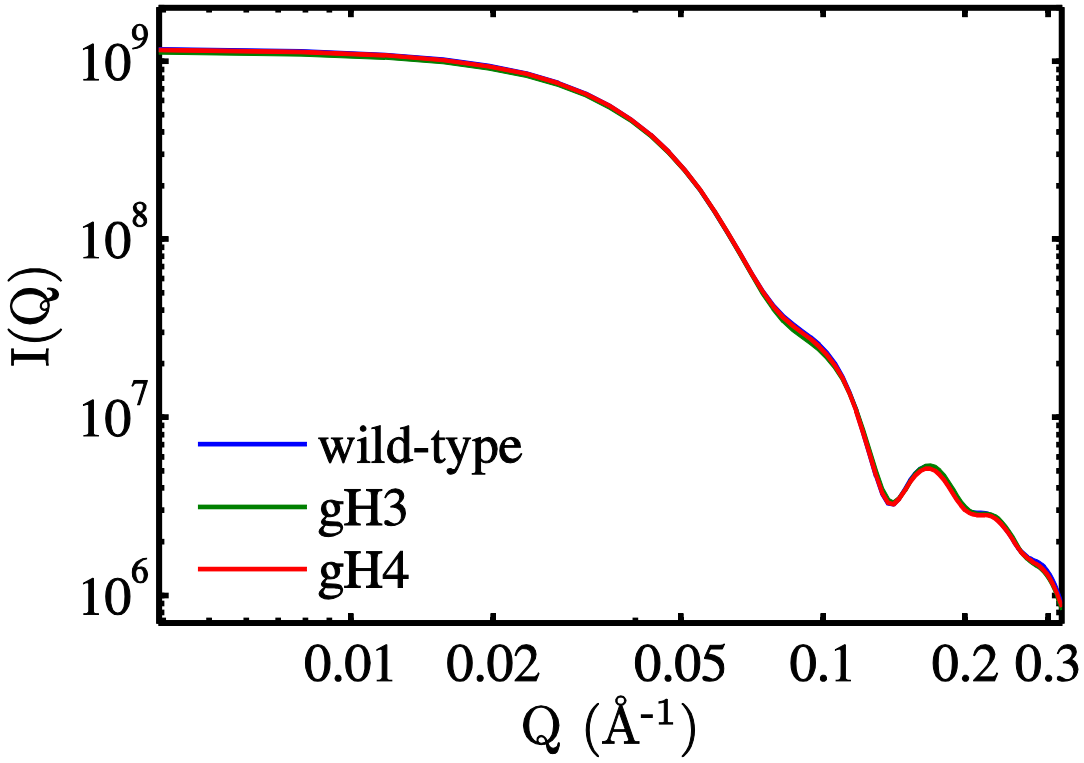


Figure S2. The form factors for the nucleosome constructs in this study. The SAXS profiles are calculated based on the nucleosome crystal structure (1KX5) using Crysol [1]. Atomic structures for the histone-tail-deletion constructs (i.e., gH3 and gH4 NCPs) are obtained by manual removal of the residues in accord with the constructs. The wild-type curve is used as the form factor for the NS-NCP and RC-NCP (results from the latter are shown in Suppl. Fig. S5). Comparisons of the three form factors indicate that tail deletions lead to rather small changes to the shape of the SAXS profile.

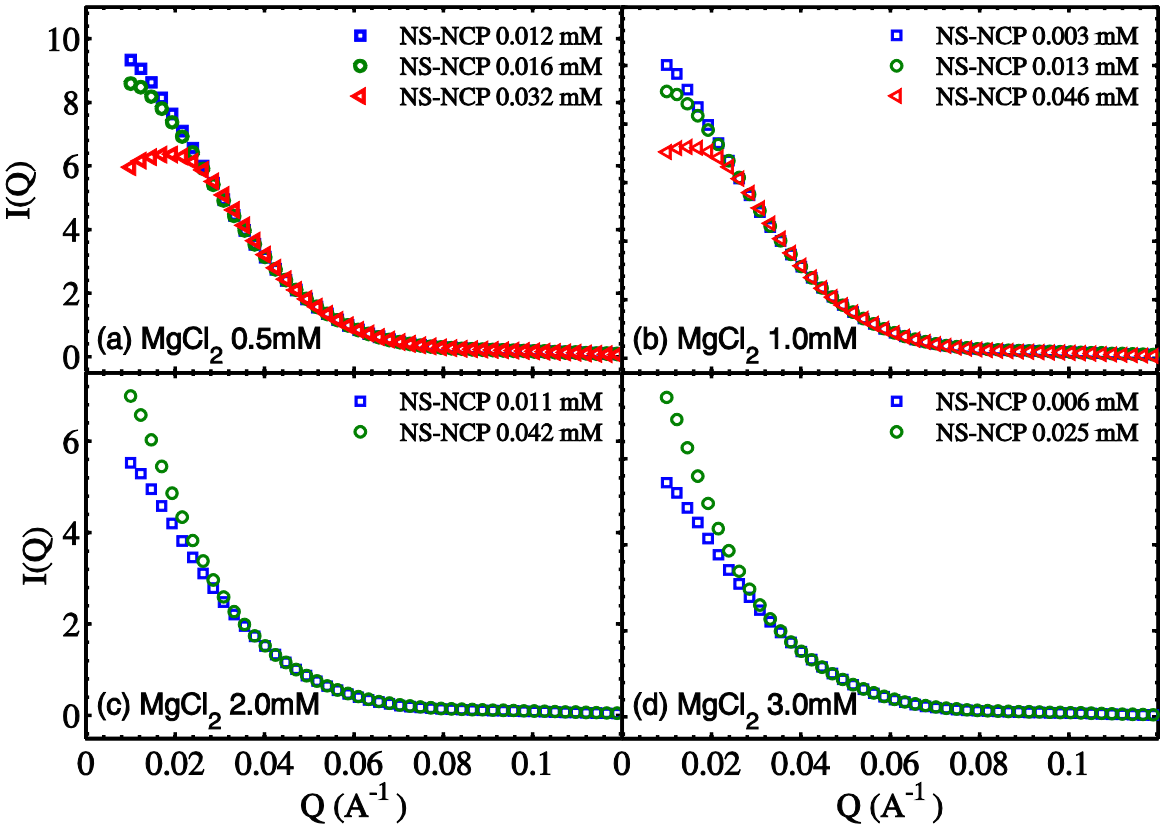


Figure S3. SAXS profiles of NS-NCPs in a series of $MgCl_2$ concentrations (no theoretical fits). Inter-NCP repulsions (low Q downturn) were observed at 0.5 and 1.0 mM $MgCl_2$, while attractions (low Q upturn) were observed at 2.0 and 3.0 mM $MgCl_2$. We have not been able to obtain satisfactory fits to the full SAXS profiles in $Mg^{2+}$ salts using the Generalized One Component Method (GOCM). We do not yet know the reasons. One speculation is that the short-range inter-NCP interactions become strongly anisotropic in $Mg^{2+}$ salts and the GOCM fails, or that there exist oligomeric states of NCPs in the presence of $Mg^{2+}$. Still, the qualitative observations of inter-NCP interactions (i.e., repulsion vs attraction) hold. Quantitative modeling of the SAXS data in $Mg^{2+}$ salts is being actively pursued in our groups.

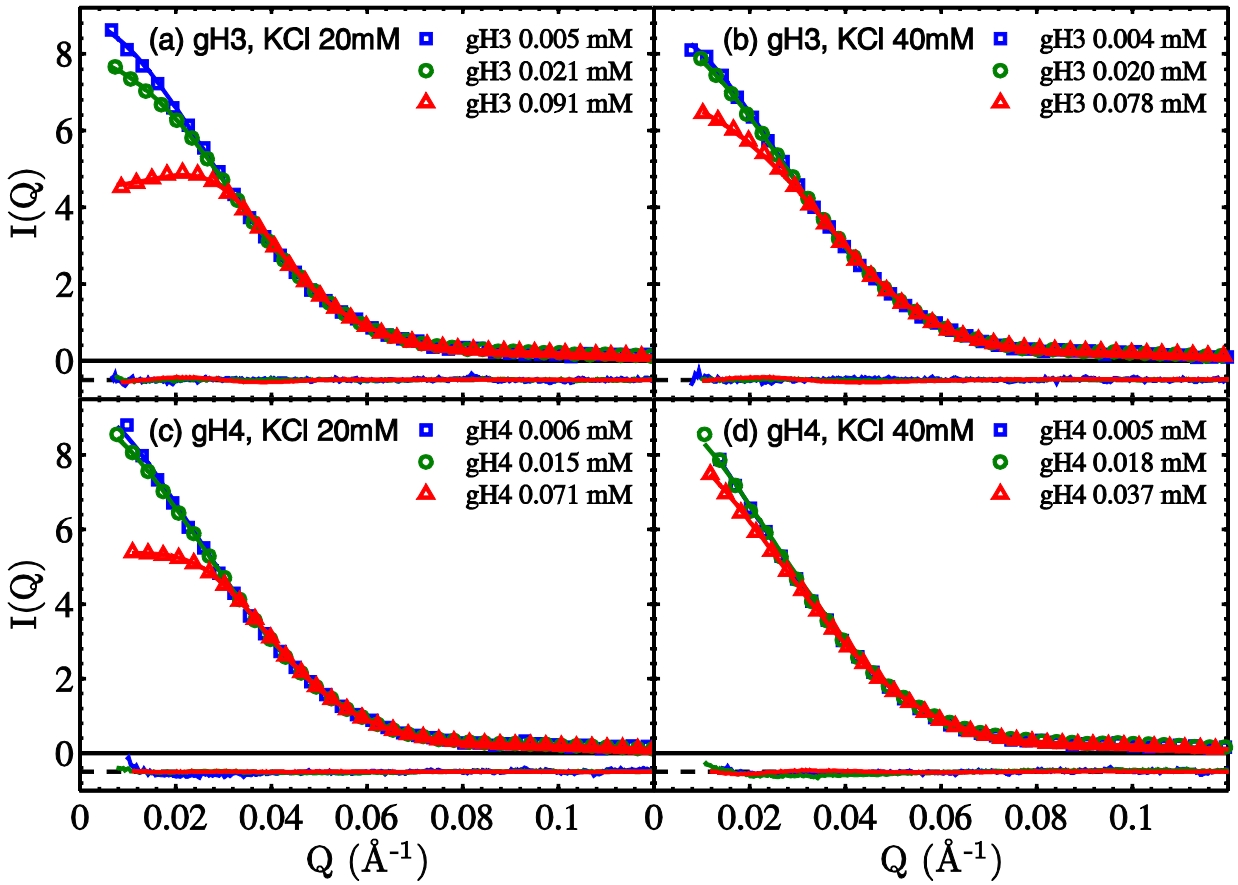


Figure S4. SAXS profiles and GOCM fits of gH3 and gH4 RC-NCPs at 20 and 40 mM KCl. I(Q)s are normalized by NCP concentrations to assist visual comparison. Each panel shows experimental I(Q)s (symbols) at a series of [NCP]s as indicated in the legends, together with their respective theoretical fits (lines). The residues are shown with an offset at the same scale. The pertinent pair-potential parameters are (discussed in detail in the main text), (a) $Z_{eff}$ = 22(1) e, σ=130 Å; (b) $Z_{eff}$ = 21(1) e, σ=110 Å; (c) $Z_{eff}$=23(1) e, σ=130 Å; (d) Unreliable fitted values due to the relative low [NCP]s and thus not given.

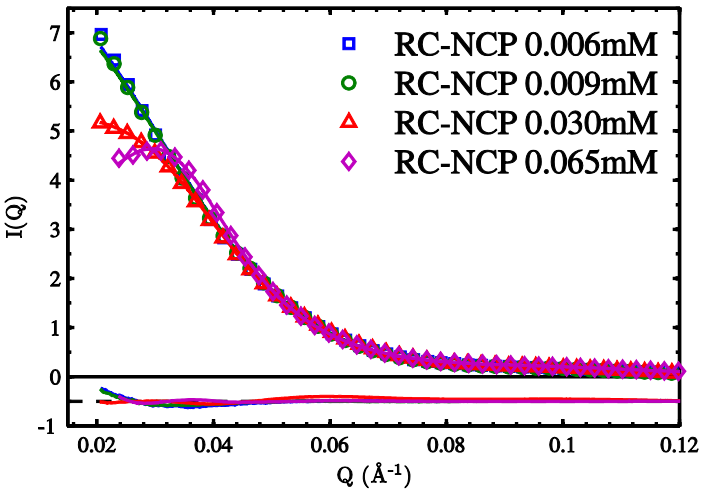


Figure S5. SAXS profiles and GOCM fits of intact recombinant RC-NCPs in 10 mM KCl. Annotations follow that of Fig. S4. The pair-potential parameters are, $Z_{eff}$ =21(1) e, σ=140 Å.

**II. Modeling the structure factor with a two-DH inter-NCP interaction potential**

In addition to the use of either repulsive or attractive Debye-Huckel (DH) potential to fit the structure factor as in the main text, the inclusion of both DH terms in the inter-NCP potential was presented here. This potential takes the form below (the same as in the main text),

$$U(r)=\begin{cases}\infty & r<\sigma \\ \dfrac{Z_{eff}^2}{\varepsilon(1+\kappa\sigma/2)^2}\dfrac{e^{-\kappa(r-\sigma)}}{r}-\dfrac{Z_{attr}^2}{\varepsilon(1+\kappa_{attr}\sigma/2)^2}\dfrac{e^{-\kappa_{attr}(r-\sigma)}}{r} & r\geq\sigma\,.\end{cases}$$

Here the hard-core potential has a fixed diameter of σ=100 Å for all samples; the electrostatic repulsive DH term has Debye length (1/κ) given by the ionic strength; and the attractive DH has decay length ($1/\kappa_{attr}$) fixed as 4.8 Å, equivalent to the Debye length at 400 mM monovalent salt. It should be noted that, as we don't know the exact nature of the inter-NCP attraction, the choice of a DH potential for inter-NCP attraction is convenient due to the available computational methods [2] but somewhat arbitrary. The choice of 4.8 Å Debye length is due to the most likely short-range nature of inter-NCP attraction, the observation of inter-molecular attractions of 4.8 Å decay length between various types of molecular surfaces[3], and the necessity of significant differences from the Debye length of the repulsive DH term in salt conditions from 10 to 200 mM KCl.

This leaves two fitting parameters in the inter-NCP potential, the effective charges of the repulsive ($Z_{eff}$) and attractive ($Z_{attr}$) DH terms. However, one complication is that there exists significant correlation between the two fitting parameters, particularly at high salts when their Debye lengths are close. This is because of the mutual cancellation effects of the two potentials. For this reason, while excellent fits were obtained (not shown), correlations between $Z_{eff}$ and $Z_{attr}$ values were evident from their fluctuations from sample to sample. To avoid such large fluctuations and facilitate comparisons between different salt conditions, we made one assumption that the attractive potential for each NCP construct (i.e., NS, gH3, or gH4 NCP) is independent of ion condition, i.e., the same $Z_{attr}$ used for all salt conditions. The $Z_{attr}$ value for each construct was determined by averaging the fitted $Z_{attr}$ values at different salts for the particular construct. This procedure led to decreases of the fitting qualities, though rather satisfactory agreements with experimental data were obtained for all samples.

We show the fitted results based on the procedure discussed above in Figures S6-9 and the fitted potential parameters in Table S1. Compared with the fits with one DH-term potential discussed in the main text, the decrease of fitting quality is more significant for the more concentrated NCP samples. As the attractive DH term is present at all salt conditions, the fitted repulsive effective charges, $Z_{eff}$, are larger than those obtained with the one-DH repulsive potential as expected. The effective charges (<50 e) are still substantially smaller than the bare charge (~150 e) or the theoretical renormalized charges (>100 e). Qualitative comparisons are thus unchanged, while the fitted inter-NCP potentials are changed quantitatively as given in Table S1. For the attractive DH term, this fitting procedure obtains the effective charge $Z_{attr}$ of 200, 165, and 154 e for the NS, gH3, and gH4 NCPs respectively. This is consistent with the results from one-DH potential fits indicating decreased attraction with tail deletions.

Overall, the inclusion of a persisting attractive term is intellectually pleasing as inter-NCP attraction (e.g., mediated by histone tails) is very likely present at all times, though overwhelmed by electrostatic repulsion at low salts. However, simultaneous determinations of both repulsive and attractive contributions are challenging.

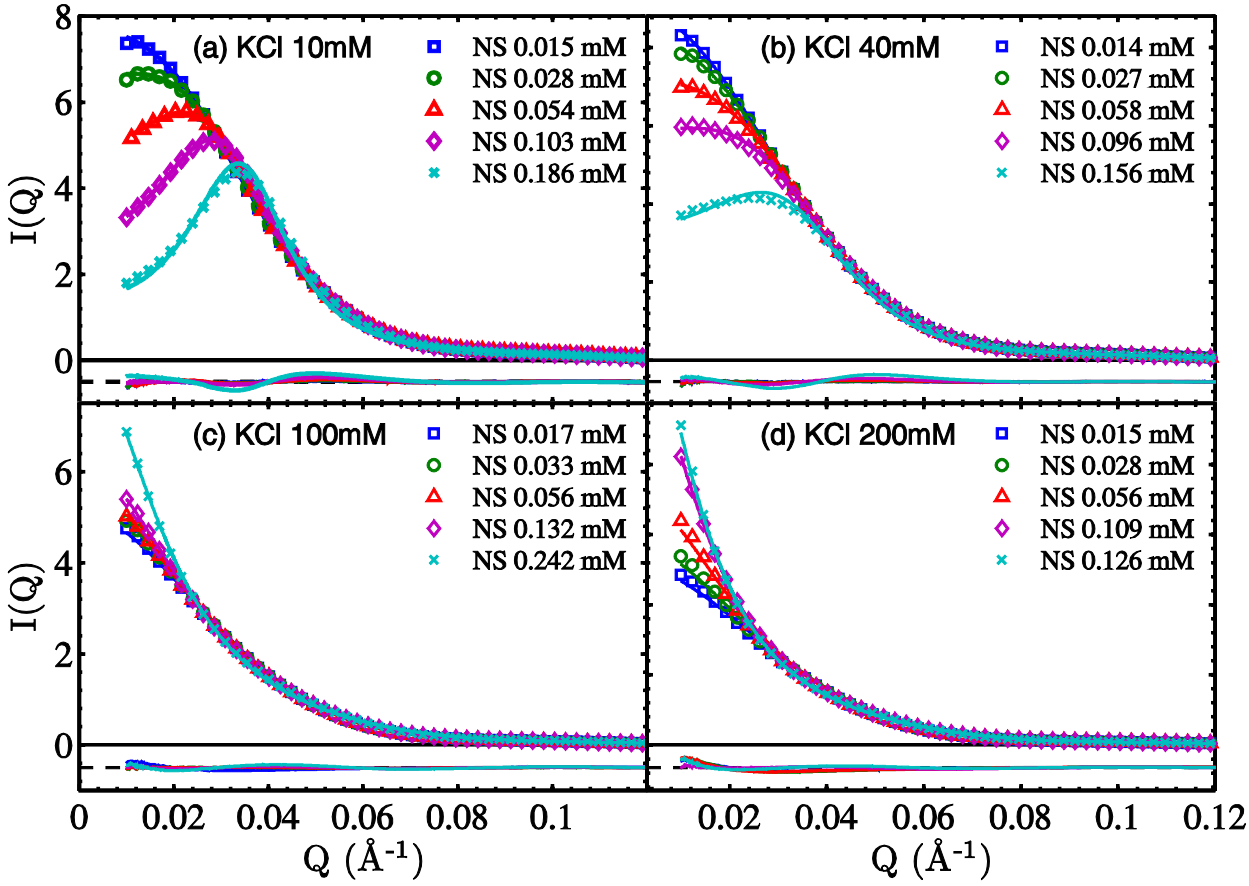


Figure S6. SAXS profiles of NS-NCP at four KCl concentrations together with fits based on the two-DH inter-NCP potential. Annotations are the same as in Fig. 2 in the main text.

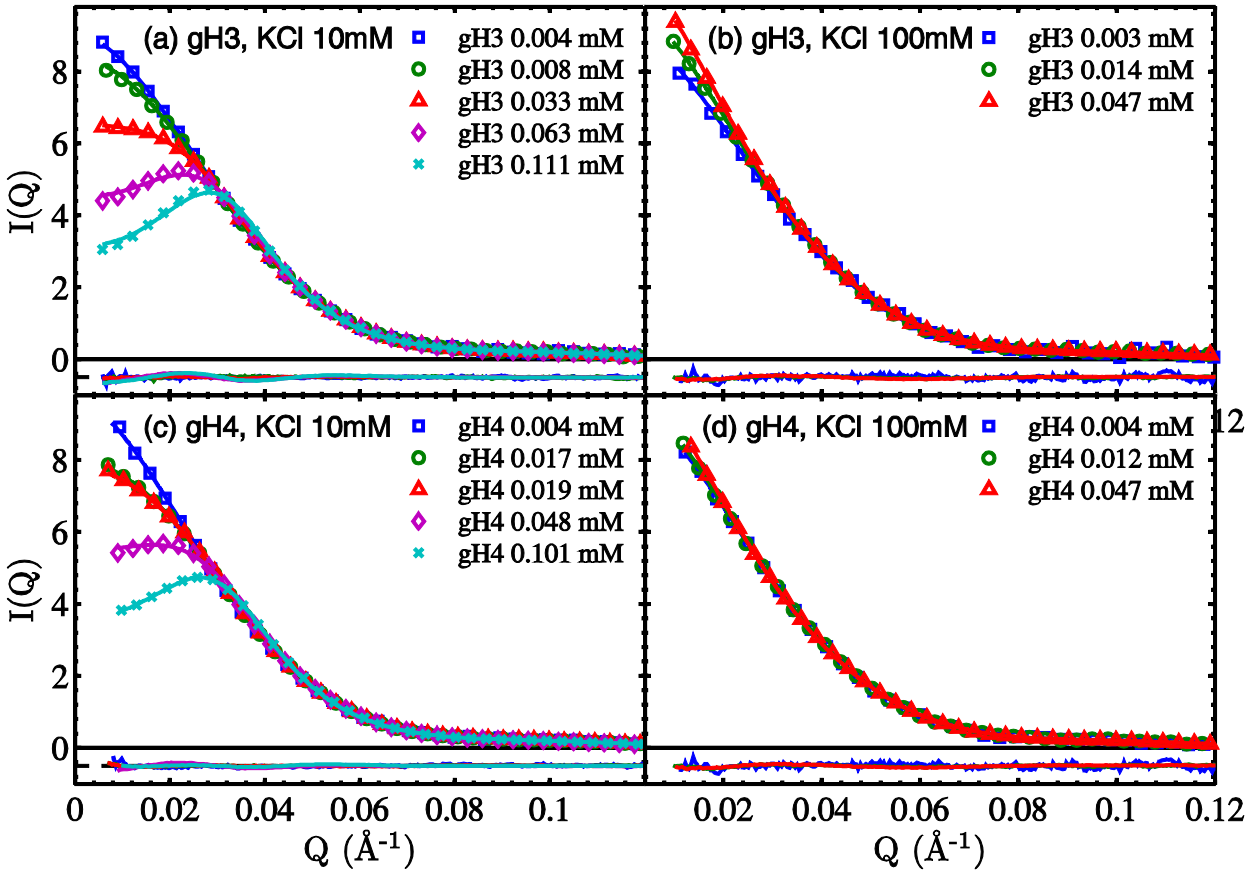


Figure S7. SAXS profiles of gH3 and gH4 NCPs at 10 and 100 mM KCl together with fits based on the two-DH inter-NCP potential. Annotations are the same as in Fig. 3 in the main text.

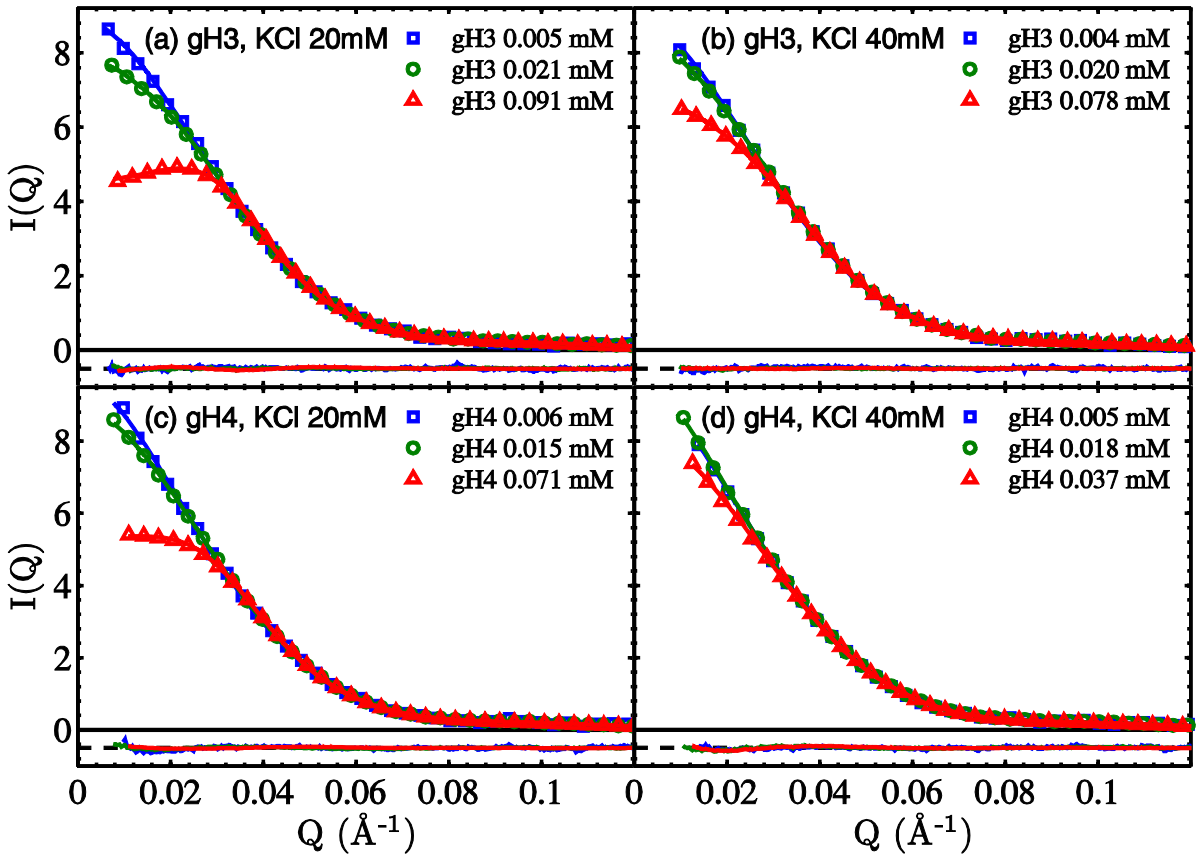


Figure S8. SAXS profiles of gH3 and gH4 NCPs at 20 and 40 mM KCl together with fits based on the two-DH inter-NCP potential.

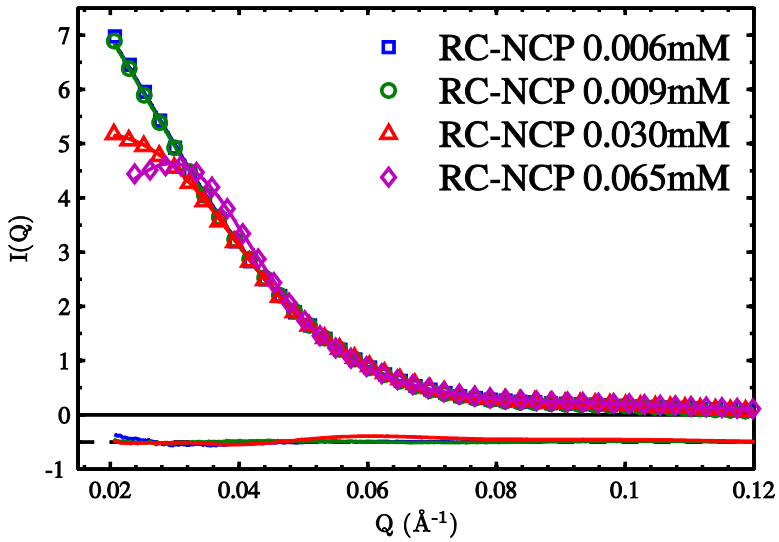


Figure S9. SAXS profiles of RC-NCPs at 10mM KCl together with fits based on the two-DH inter-NCP potential.

Table S1. Inter-NCP interaction parameters from structure factor fittings with either one-DH potential (in the main text) or two-DH potential (in the Supplemental Data). As the structure factors are more pronounced at high NCP concentrations, the values in this Table are taken as the mean over the 2-3 most concentrated samples for which the fits are the most reliable. For the fits with one DH term in the inter-NCP potential, the fitted effective charge ($Z_{eff}$ or $Z_{attr}$) shows no systematic trends with the NCP concentration. For the fits with two DH terms, the fitted effective charge ($Z_{eff}$) generally increases slightly with the increase of the NCP concentration. We do not know the reason for the different trends from fitting the same data and speculate that this may arise from how the generalized one component method handles the effects of sample concentration with or without an attractive term [4]. Note the values for the gH4-NCP construct at 40 mM KCl are unreliable due to the relative low [NCP]s.

| | | One-DH inter-NCP potential | | | Two-DH inter-NCP-potential | | |
|---|---|---|---|---|---|---|---|
| NCP construct | [KCl] (mM) | σ (Å) | $Z_{eff}$ (e) | $Z_{attr}$ (e) | σ (Å) | $Z_{eff}$ (e) | $Z_{attr}$ (e) |
| NS-NCP | 10 | 140 | 22(1) | 0 | 100 | 35(4) | 200 |
| | 40 | 110 | 23(1) | 0 | 100 | 49(6) | 200 |
| | 100 | 100 | 0 | 150(5) | 100 | 45(8) | 200 |
| | 200 | 100 | 0 | 200(8) | 100 | 1(1) | 200 |
| gH3-NCP | 10 | 140 | 21(1) | 0 | 100 | 31(3) | 165 |
| | 20 | 130 | 22(1) | 0 | 100 | 38(3) | 165 |
| | 40 | 110 | 21(1) | 0 | 100 | 48(4) | 165 |
| | 100 | 100 | 0 | 123(4) | 100 | 23(4) | 165 |
| gH4-NCP | 10 | 140 | 20(1) | 0 | 100 | 30(3) | 154 |
| | 20 | 130 | 23(1) | 0 | 100 | 33(3) | 154 |
| | 40 | -- | -- | -- | -- | -- | -- |
| | 100 | 100 | 0 | 100(4) | 100 | 30(10) | 154 |
| RC-NCP | 10 | 140 | 21(1) | 0 | 100 | 34(3) | 200 |

1. Svergun D, Barberato C, Koch MHJ. *Crysol - a Program to Evaluate X-Ray Solution Scattering of Biological Macromolecules from Atomic Coordinates*. **J Appl Crystallogr**. 1995;28:768-73.
2. Liu Y, Chen W-R, Chen S-H. *Cluster Formation in Two-Yukawa Fluids*. **The Journal of Chemical Physics**. 2005;122(4):044507.
3. Zemb T, Parsegian VA. *Editorial Overview: Hydration Forces*. **Current opinion in colloid & interface science**. 2011;16(6):515-6. PMID: ISI:000298523900009.
4. Chen SH, Sheu EY, Kalus J, Hoffmann H. *Small-Angle Neutron-Scattering Investigation of Correlations in Charged Macromolecular and Supramolecular Solutions*. **J Appl Crystallogr**. 1988;21:751-69.